# RSRE
# MEMORANDUM No. 4128

# ROYAL SIGNALS & RADAR ESTABLISHMENT



## A THEORETICAL AND EXPERIMENTAL INVESTIGATION INTO THE USE OF SAW WEIGHTING TECHNIQUES IN OPTICAL DIFFRACTION GRATINGS

Authors: M F Lewis and C L West



PROCUREMENT EXECUTIVE,
MINISTRY OF DEFENCE,
R S R E MALVERN,
WORCS.

ROYAL SIGNALS AND RADAR ESTABLISHMENT

MEMORANDUM NUMBER 4128

TITLE: A THEORETICAL AND EXPERIMENTAL INVESTIGATION INTO THE USE OF SAW WEIGHTING TECHNIQUES IN OPTICAL DIFFRACTION GRATINGS

AUTHORS: M F Lewis and C L West

DATE: March 1988

## SUMMARY

This memorandum describes the behaviour of optical diffraction gratings which have been weighted in various ways analogous to those used in surface acoustic wave (SAW) devices. It is shown experimentally and theoretically that a wide variety of two-dimensional responses can be achieved by these means. In this study we have chosen to concentrate on quasi-rectangular responses, and we describe in some detail the factors that limit the performance achievable in practice. Some possible applications of these techniques in the spatial, temporal and spectral domains are mentioned. A succinct version of this memorandum has been accepted for publication in the journal "Applied Optics" (probably the June 1988 edition).

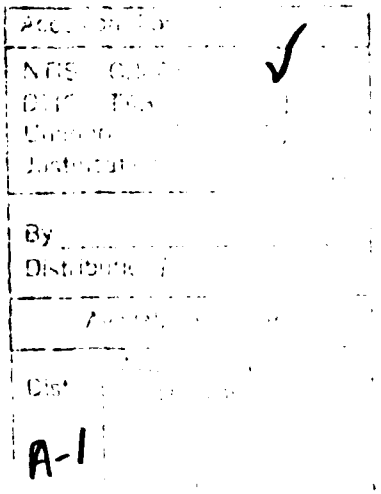




# 1 INTRODUCTION

An ideal transmission optical diffraction grating comprises a large number of identical parallel equispaced slits in an otherwise perfectly opaque planar screen. The behaviour of such a device when illuminated with an optical plane wave forms a classical study which is commonly used for tutorial purposes, while practical derivatives in the form of reflection and transmission gratings incorporating blazing, etc, have long been exploited, for example in monochromators and spectrometers[1-4]. Although it is self-evident that such a grating and its output are 2-dimensional (2-D), the conventional treatment is often 1-dimensional (1-D), and effectively assumes that the grating is employed in conjunction with a point detector located on an axis of symmetry in the focal plane of a subsequent lens ($L_3$ in Figure 1a), when the response comprises a number of grating orders, each of sinc-function form[5]. The relative amplitudes of these orders depend on the slit width[1-4], for example the even orders, except the zeroth, are absent for equal slit and gap widths. (In antenna theory these features are known as the array factor and element factor respectively.) Few variations on this arrangement have been described in the literature, the most common being deliberate or accidental *apodization* through the use of an input optical beam with a Gaussian spatial profile, when the responses of the individual orders tend towards a Gaussian form, ie having no sidelobes as such, but comprising a broader central peak with monotonically decaying wings[2,3].

An *acoustic* component closely analogous to the optical diffraction grating is the interdigital transducer (IDT) which in its basic form comprises a large number of parallel linear equispaced sources of acoustic waves, usually surface acoustic waves, SAW. By analogy with the optical diffraction grating, the acoustic frequency response of such a transducer is of sinc-function form. However, in contrast to the optical diffraction grating, the IDT has been modified in numerous ways in recent years to achieve many desirable frequency responses for use in electronics[6-8], the basic sinc-function response itself rarely being of interest. For example, weighting procedures have been devised to provide $\geq$ 60 dB frequency-domain sidelobe suppression in bandpass filters, while chirped IDTs (transducers with monotonically varying spatial period) are regularly employed in spectrum analysis, and in pulse compression radar for waveform generation and matched filtering. One particularly valuable feature of SAW devices is the close resemblance between the physical structure of a weighted IDT and its (temporal) impulse response, h(t), from which the frequency response, H(f), can be obtained by Fourier Transformation; an analogous behaviour obtains in the weighted optical diffraction gratings described below. For the convenience of readers unfamiliar with SAW device technology a succinct summary of its principal attributes is included in Appendix 1. In this memorandum we describe the results of an investigation into the use of such IDT weighting techniques in optical diffraction gratings. Many phenomena familiar to the SAW community are reproduced in the optical devices, but several new effects also appear. For example, weighted optical diffraction gratings display an apparently anomolous behaviour in their zeroth and even orders, which effects are not encountered in SAW devices since they do not respond at their zeroth or even harmonics. Further, as shown later, the 2-dimensionality of the output field can hardly be ignored in weighted optical diffraction gratings, whereas almost all SAW device designers have striven to avoid this aspect of their devices, as discussed in Appendix 1. Ironically it is only recently that the benefits of exploiting the second dimension in SAW devices have been recognised, and then often by analogy with optics![9,10] In the next section of this paper the behaviour of a conventional optical diffraction grating is reviewed, not by the usual phasor summation procedures, but rather by using the languages of (a) Fourier optics[11], and (b) temporal impulse responses, as this forms convenient groundwork for the analysis of the weighted gratings discussed in sections 3 and 4.

## 2 THEORETICAL AND EXPERIMENTAL RESPONSES OF A CONVENTIONAL OPTICAL DIFFRACTION GRATING

It is convenient to begin by recalling that if an aperture is illuminated normally by a monochromatic plane wave the far-field (Fraunhofer) pattern is proportional to the Fourier Transform (FT) of the field in the aperture plane[2,11]. In practice it is usual to image this far-field pattern on to a convenient measurement plane, eg by using lens $L_3$ in Figure 1a. If the separations of the grating and output plane from the lens, $L_3$, are each made equal to the focal length, $f_o$, as in Figure 2, then the FT relationship again obtains in both amplitude and phase[11]. Thus the (complex) amplitudes in the input (x,y) and output (u,v) planes are related by

$$F(u,v) = \iint dxdy\ f(x,y)\ \exp\left[\frac{-j2\pi}{\lambda f_o}(ux+vy)\right] \qquad (1)$$

The factor $(1/\lambda f_o)$ in the exponent shows that the scale in the output plane depends on $f_o$, the focal length of the lens, and on $\lambda$, the optical wavelength. For simplicity we follow the common practice of dropping this factor. This is also a particularly convenient simplification in the case of the modified arrangement of Figure 1b in which an adjustable scale factor obtains as discussed in reference (12), and Appendix 2.

It may be noted that most detectors are insensitive to optical phase and respond only to the intensity I (u,v) where

$$I(u,v) = \left|F(u,v)\right|^2 \qquad (2)$$

Consequently if the output plane in Figures 1a and 2 is a detector plane the distance from the input plane (grating) to the FT lens becomes immaterial. This point is best appreciated by noting that each plane wave component deriving from the diffraction grating focusses at a point in the focal plane dependent only on the orientation of its k-vector relative to the optical axis. Moving the grating axially only affects the optical phase by modifying the pathlengths of the plane wave components.

In the experiments described below we have further modified the geometry to that shown in Figure 1b, in which the Fourier Transformation is performed by lens $L_2$. This configuration is preferred as it employs a smaller number of optical elements, and is readily adjusted to magnify the output plane so as to fill the aperture of the camera. The concomitant distortion of the optical phase in the output plane is again irrelevant in our measurements. The overall behaviour of the arrangement of Figure 1b is derived in Appendix 2.

The field in the output plane of a conventional optical diffraction grating measurement (Figures 1a or 2) can be derived from Equation 1 by noting that the grating can be generated from 3 terms:

a. the rectangular aperture function

$$f_1(x,y) = f_2(x)f_3(y) = \prod\left[\frac{x}{a}\right]\prod\left[\frac{y}{b}\right] \qquad (3)$$

where, following Bracewell[13], the rectangular function $\prod(x)$ is defined by

$$\prod(x) = 0 \quad \text{if } |x| > \frac{1}{2}$$
$$\prod(x) = 1 \quad \text{if } |x| < \frac{1}{2} \qquad (4)$$

b. a 'picket fence' in the x-direction with period, p,

$$f_4(x) = \sum_{n=-\infty}^{\infty} \delta(x-np) = \left[\frac{1}{p}\right] III\left[\frac{x}{p}\right] \qquad (5)$$

where the shah function III may conveniently be defined by[13]

$$III(ax) = \frac{1}{|a|} \sum_{n=-\infty}^{\infty} \delta\left[x-\frac{n}{a}\right] \qquad (6)$$

in which a is an arbitrary constant and $\delta$ is the Dirac delta-function,

c. the rectangular profile of an individual slit of width, W, in the x-direction.

$$f_5(x) = \prod\left[\frac{x}{W}\right] \qquad (7)$$

The structure of the grating of Figure 2 is given by

$$f(x,y) = (f_1 x f_4) * f_5 \qquad (8)$$

where x denotes multiplication and * denotes convolution[13]. Using the convolution theorem, the Fourier Transform of f(x,y) is immediately given by

$$F(u,v) = (F_1 * F_4) x F_5 \qquad (9)$$

which is straightforward to calculate as it conveniently separates in x and y:

$$F(u,v) = [\{a\ sinc(au)\ b\ sinc(bv)\} * III(pu)]\ x\ W\ sinc(uW) \qquad (10)$$

where

$$sinc(x) = \frac{\sin(\pi x)}{\pi x} \qquad (11)$$

The first term on the rhs of Equation 10 represents the conventional sinc-function response of the grating, while the second term describes a sinc-function in the v-direction which is usually ignored. The III-function generates the multiple grating orders, and the final sinc-function is the envelope of the amplitudes of the various orders. The expression in Equation 10 is equivalent to the conventional grating response derived, for example, in reference (1). Clearly the normally-cited sinc-function response of a conventional optical diffraction grating arises from the aperture function, $f_2(x)$ alone. For future reference it is useful and instructive to derive this preliminary result in an alternative manner. Recalling from an earlier footnote the close relationship between the grating responses in the spatial and frequency domains let us derive the temporal impulse response, h(t), of the arrangement of Figure 2. This is the response measured by an ideal point detector located at ($u = f_0 \sin\theta$, $v = 0$) to an input optical plane wave of infinitely short duration, viz a Dirac delta function, $\delta(t)$. It is self-evident from Figures 1a and 2 that h(t) comprises N rectangular functions (one from each slit) each of duration $\Delta = |W\sin\theta/c|$, and incrementally delayed by $\tau = |p\sin\theta/c|$, where c is the velocity of light. The overall amplitude varies as $|\mathrm{cosec}\theta|$ being inversely proportional to the duration $\Delta$. Thus

$$h(t) \propto |\mathrm{cosec}\theta| \left[ \Pi\left(\frac{t}{T}\right) \times \frac{1}{\tau} \mathrm{III}\left(\frac{t}{\tau}\right) \right] * \Pi\left(\frac{t}{\Delta}\right) \qquad (12)$$

where $T = N\tau$, and where we have shifted the origin of time to the centre of h(t) for convenience. The response at an optical frequency, f (= $c/\lambda$), is therefore

$$H(f) \propto |\mathrm{cosec}\theta| \left[ T\ \mathrm{sinc}(fT) * \mathrm{III}(f\tau) \right] \times \Delta\ \mathrm{sinc}(f\Delta) \qquad (13)$$

The first sinc-function in Equation 13 is consistent with that in Equation 10, recalling the earlier omission of the factor $1/\lambda f_0$ from u, and each response is implicitly a function of both u and $\lambda$. The shah-function in Equation 13 generates the multiple grating orders (eg defined by the wavelengths of the principal maxima) obtaining at a given $\theta$, and the relative amplitudes of these orders are determined by the final sinc-function. Again it is clear that the classical sinc-function response derives from the aperture function of the grating, and it is this function that is modified in the next section of the paper to derive new responses. Before describing this, however, it is necessary to mention two further modifications to the experimental arrangement that we have used to improve the dynamic range of certain measurements. The basis of these techniques is to convert the optical measurements to the electrical domain and thereby exploit the logarithmic response and massive dynamic range of modern electronic equipment, specifically the Hewlett-Packard 8505A network analyser. When using these schemes the camera of Figure 1a was replaced by a 'point' detector whose area was defined by a 50 $\mu$m pinhole, the combined "pinhole plus detector" being mechanically translated relative to the output plane. The simpler technique was used in preliminary studies only, and employed an acoustic Bragg cell to amplitude-modulate the laser output at a convenient rf frequency ($\sim$ 20 MHz) derived from the network analyser, and feeds the output of the optical detector back into the network analyser. In our experiments this provided a logarithmic output with an undistorted 35 dB optical dynamic range. (In these measurements the display of the network analyser is modified by a factor of 2 in dBs through the use of a square-law optical detector.) While this technique proved invaluable, some of the results presented in this memorandum display a superior dynamic range of $\sim$ 45 dB. This was achieved by using a more complicated heterodyne technique in which a frequency-shifted optical local oscillator beam is generated in the Bragg cell and mixed with the unshifted signal beam at the detector (by the use of beam splitters). In this latter scheme the output rf level is a function of the signal amplitude rather than intensity and should therefore display approaching twice the dynamic range (measured in dBs) of the aforementioned direct detection scheme. However in practice the dynamic range realised was limited to $\sim$ 45 dB by optical scatter in the Bragg cell, this value also being typical of acousto-optic spectrum analysers. It could possibly be improved further by using a Bragg cell operating in the anisotropic mode together with polarisers to separate the deflected and scattered light[14], or another modulation technique altogether, eg electro-optic. Figure 3 demonstrates the capability of the heterodyne technique by comparing the measured response of a conventional chrome-on-glass diffraction grating (of 200 slits, 16 $\mu$m period and nominally 1:1 mark/space ratio) in its first grating order, with theory over a dynamic range of 45 dB. The optical source used in this measurement and in all others of this paper unless otherwise stated is an Argon ion laser operating at $\lambda$ = 514.5 nm.

## 3. WEIGHTED DIFFRACTION GRATINGS

In this section we describe the modification of the aperture function of a diffraction grating to provide a response of nominally 'top-hat' or rect-function form, Equation (4). This form was chosen as it could be of value in the spectral or spatial domains, while the generalisation of our procedures to other functions is entirely straightforward, being based on Fourier Transform theory. It is clear from the preceding section that to obtain a rect-function response requires an aperture function equal to the (inverse) FT of the rect-function, ie of sinc-function form, Equation (11). Unfortunately, however, this cannot be realised exactly for two reasons. Firstly the sinc-function is of infinite extent,

and so must be truncated in practice; as shown later this results in some degree of in-band ripple, and the appearance of out-of-band sidelobes (eg Figures 5 and 6 later). The extent of these deviations depends on the manner of truncation. Secondly it should be noted that the sinc-function changes sign in alternate sidelobes and this precludes implementing a rect-function response in the zeroth grating order unless one resorts to sophisticated techniques such as evaporating a dielectric layer of approproate thickness over the negative slits. However if we initially confine our attention to the ± 1 grating orders we can resort to the SAW technique of shifting the slit locations by half a period to implement the required change in sign[6-8,15]. This procedure is equivalent to the optical 'detour phase' technique[16], and in this section we describe its use in conjunction with apodization and withdrawal-weighting.

a. Apodized Gratings

In this technique the weighting is implemented by varying the lengths of the slits[17]. A series of seven patterns employing apodization has been designed and tested. These patterns all include the main lobe of the sinc-function, together with a symmetrical sidelobe pattern containing on each side m = 0, ½, 1, 1½, 2, 2½ and 3 sidelobes respectively. One such slit pattern with m = 1½ is illustrated in Figure 4a. As in the conventional (comparison) grating of Figure 3 the period p = 16 $\mu$m, the slit and gap widths each being nominally 8 $\mu$m. This is sufficiently large to avoid any polarisation-dependent phenomena which arise when the slit width is of the order of the optical wavelength, $\lambda$[4]. The main lobe contained 200 slits giving each quasi-rectangular response a fractional full-width of 1%. Figures 5a and b show the calculated responses, and those measured along the symmetry axis of the output plane (corresponding to v = 0 in Figure 2). These measurements are on a linear optical power scale and show excellent agreement between the measured and calculated levels of the in-band ripple. Figure 5a shows that as more sidelobes are retained in the grating, more ripples appear across the passband. For integer values of m the total number of ripples is 1 + m. It is in this sense that the overall response approaches a rectangular function with increasing m, but strong ripples always remain at the band edges if the grating patterns are truncated sharply, as here. Perhaps more surprising at first sight is the fact that the passband is generally flatter for patterns truncated half-way through the outer sidelobes (eg Figure 4a) than for those truncated at a null between sidelobes. The explanation of this is given below, where it is shown that this improved response in-band is accompanied by a higher spurious sidelobe level out-of-band. Experimental confirmation of this latter feature appears in Figure 6 where we have used the network analyser technique of section 2 to present results on a dB scale. This figure illustrates the relatively high sidelobe levels[18] of the grating patterns with half-integer sidelobes[18], but it may be noted that the measured levels are a little higher than calculated, possibly due to slight overlap of the detector with the off-axis sidelobes of apodised gratings (see later, eg Figure 8). This behaviour can be explained graphically with the aid of Figure 7. The top of this figure shows that a truncated sinc-function, a, can be regarded as the product of a complete sinc-function, b, and a rect-function, c. Below this (d-f), is shown the corresponding picture in the FT domain, in which multiplication is replaced by convolution. Thus the overall response, d, can be visualised[2,13] as arising by reversing one function (say f, which is unnecessary as it is symmetrical) and running it through e, the product of these functions being integrated to form an instantaneous value of d. As illustrated in Figure 7g and 7h the in-band response obtains as the main lobe of f traverses the non-zero part of e, the in-band ripple arising from the entry and exit of the sidelobes of f. Now it is readily shown that for patterns with an integer number of sidelobes, a positive sidelobe of f enters e as a negative sidelobe leaves e (etc) leading to a strong ripple, Figure 7g. The opposite is true of a pattern containing a half-integer number of sidelobes in which the entry of a positive sidelobe is accompanied by the exit of a positive sidelobe (etc), leading to relatively little ripple, Figure 7h. Similarly, each of these behaviours is reversed out-of-band, Figures 7i and 7j, which is a simple consequence of the fact that the main lobe of the sinc-function is twice as wide as each

sidelobe, eg see Figure 3. Thus there is a trade-off between the in-band response and the out-of-band response. Although this behaviour is also an inherent feature of SAW filters the authors are unaware of any prior recognition of it; in practice SAW device designers use computer procedures which optimise the overall performance numerically, at the expense of physical insight.

There are two other aspects of the responses of apodised diffraction gratings that are worthy of comment, namely the 2-dimensionality of the optical field in the output plane, and the behaviour of the grating in the zeroth and even orders. These are now discussed in turn. The results presented so far have described the behaviour of the output field on the symmetry axis (v = 0) of the output plane. An isometric view of the intensity across the full 2-dimensional output plane, (u,v), is shown in Figure 8a, together with a calculated version derived from Equations (1) and (2) using the actual apodised grating slit pattern for f(x,y). Obviously the detailed agreement is gratifying but otherwise there are only two minor points of interest. Firstly, the function f(x,y) is no longer separable in x and y (as it was for a grating with rectangular aperture, Equation (3)) and so the computation was performed numerically rather than analytically. Secondly the appearance of strong 'spurious' sidelobes off the symmetry axis is very evident, making it necessary to measure accurately along the axis to obtain the low out-of-band sidelobe levels eg in Figure 6.

The behaviour of apodised gratings in the even grating orders is also of some interest. Figure 9 compares a typical zero-order pattern with the corresponding 1st order pattern; this employed an apodised grating containing m = 3 sidelobes on each side of the main lobe. The dramatic difference is readily seen to arise from the breakdown of the sign-reversal procedure described earlier, for in the zeroth order any slits anywhere in the input plane are in phase at (u = 0, v = 0), for any optical wavelength. A similar response to the zeroth order obtains in the 2nd, 4th ..... orders, if present, because the effect of the half-period step is to introduce additional pathlengths of precisely $\lambda$, $2\lambda$, etc as shown in Figure 10a. Conversely in the 3rd, 5th ..... orders the additional pathlengths generating the 'detour phase' become $3\lambda/2$, $5\lambda/2$ ..... etc, restoring the behaviour in the 1st order. Experimental confirmation of this is presented in Figure 10b. An equivalent mathematical interpretation of this effect can be derived from sampling theory. Thus in the grating patterns containing p/2-steps the basic sampling period is p/2 rather than p (many samples having zero amplitude). Hence in the convolution process of Equation (10) the fundamental response is repeated every two orders of the original grating. Thus the original odd orders (including ± 1) all behave in one manner, and the original even orders (including the zeroth) all behave in another, 'spurious', manner. (Coincidentally, if such a grating has an accurate 1:1 mark/space ratio the only 'spurious' order present is the zeroth.) Amusingly this conclusion also applies to a conventional grating with an *even* number of slits because the centre does not coincide with any slit, the slits being arrayed as a displaced shah-function, $\mathrm{III}(x/p-\frac{1}{2})$. In this case the only consequence is a change in *sign* of the amplitudes of alternate pricipal maxima, the intensities being unaffected (ref 13, p359). This may also be seen from the even number of inter-order sidelobes, which, of course, alternate in sign.

Some potential applications of weighted diffraction gratings involve the separation of different optical wavelengths in spectroscopy, wavelength division multiplexing etc. In the latter connection we included in section 2 a derivation of the frequency (wavelength) response of a conventional grating in conjunction with a fixed point detector, and showed that this mimicked the spatial response at a fixed optical wavelength. By using a dye laser we have verified the same behaviour experimentally in our weighted gratings, e.g. to generate frequency responses of the same form as the spatial responses of Figure 5. Rather than reproduce these we illustrate in Figure 11 a related phenomenon, namely the response of an apodized grating when illuminated by an argon-ion laser operating in its "all lines" mode. The responses of the 5 laser lines all appear clean, but to achieve this it was necessary to employ achromatic optics to ensure that all responses focussed in a

common plane, ie that of the camera in Figure 1b.

b. Withdrawal-weighted gratings

In this technique all the grating slits retain the same length in the y-direction, and weighting is achieved by omitting slits at appropriate locations in the grating, Figure 4b. As in the case of apodised gratings, an effective phase-reversal in the ± 1 (and all odd) grating orders can be implemented by displacing the appropriate slits by ± p/2. A set of 7 such patterns has been made for direct comparison with the apodised gratings of the previous section. These were designed with the same fractional bandwidth as the apodised grating, so that the main lobe could accommodate up to 200 slits, and each sidelobe up to 100 slits leading to a 1% full fractional bandwidth. The patterns were generated by integrating the area under the sinc-function numerically, working out from the centre. A slit was called for each time this area increased by unity. In the negative sidelobe regions, the slits were displaced by ± p/2 symmetrically with respect to the centre of the grating. The largest grating contained 118 slits in the main lobe, and 14, 8, and 6 in each successive sidelobe. These even numbers of slits made it straightforward to implement the half integer sidelobe patterns. This weighting procedure proved most successful, as can be judged from the fact that the measured and calculated grating responses, shown in Figures 5c and 5d, are barely distinguishable from those the corresponding apodised gratings in Figures 5a and 5b.

There are, however, two significant differences in the detailed behaviour. Firstly the aperture function $f_1(x,y)$ has again become separable in x and y, the y-dependence being $f_3(y) = \prod(y/b)$ as for the unweighted diffraction grating discussed in section 2. Thus the response in the v-direction of the output plane has a sinc-function variation, as shown in Figure 8b. Such a feature could be of practical benefit, as it allows the detector(s) to be extended in the v-direction, in contrast to the apodised gratings of Figures 8a. The other principal difference in behaviour of the apodised and withdrawal-weighted diffraction gratings concerns their behaviour between grating orders. In the case of the apodised gratings the response on the symmetry axis v = 0 declines dramatically between orders in a manner reminiscent of a conventional grating with a sinc-function response, Figure 12c. This is confirmed experimentally to the limit of our measurement accuracy, as shown in Figure 12d. By contrast, in the case of withdrawal-weighted gratings the sidelobe level increases greatly between orders as shown in the calculated and experimental curves of Figure 12a and b respectively. This behaviour is well-known in the discipline of the SAW bandpass filter design[19], and here we give only a physical description of its origin:- We saw earlier that the technique described for implementing sign reversals in the ± 1 grating orders is ineffective in the even orders (Figure 10) because it does not introduce a true 180° phase-shift. Instead it introduces pathlength changes equivalent to ± λ/2 at the centre frequency (wavelength) of the ± 1 grating orders. However, apart from this effect, the apodised grating is a uniformly (over-)sampled version of the sinc-function envelope, and by the sampling theorem will therefore reproduce the required bandlimited response exactly[13]. Now if we compare the physical construction of apodised and withdrawal-weighted diffraction gratings (Figure 4) we see that a withdrawal-weighted pattern could be generated from the corresponding apodised grating by moving several weak slits by integer numbers of periods, p, so as to produce a smaller number of full-length slits. Such movements are of no significance at the centre frequencies of the ± 1 grating orders as they introduce pathlength changes of an integer number of wavelengths. However at other frequencies they do affect the response. In the particular patterns described here these pathlength changes amount to several wavelengths, and so affect the response at frequencies removed from the centre of the grating order by as little as ~ 10%.

## 4. DISPERSIVE GRATINGS

In the previous section we have described the behaviour of optical diffraction gratings

weighted symmetrically (in the x-direction) using the techniques of apodisation and withdrawal-weighting to provide nominally rect-function responses. For completeness we include in this section a succinct description of the behaviour of dispersive gratings because in their usual form they also display responses of nominally rect-function form. However, as their name implies, their phase response is non-linear, ie they are dispersive.

Dispersive gratings are designed so that the period, p(x), varies across the grating, usually in a monotonic manner as shown schematically in plan view in Figure 13a. For simplicity we assume that the slits are all present and of the same length in the y-direction, resulting in the previously described sinc-function response in the v-direction of the output plane. It may be noted, however, that apodisation and withdrawal-weighting provide convenient amplitude-weighting techniques in dispersive gratings, if required. The most commonly described devices of this type are linear chirp gratings, in which the spatial frequency (which is inversely proportional to the local period, p(x)) varies linearly across the grating. A potentially useful aspect of such devices is their ability to form a focus in the near/intermediate field; this is denoted by F in Figure 13a. Travelling acoustic wave versions of such gratings have been proposed for use in signal processing[20,21] and as flying line or spot scanners e.g. in laser printing or displays[22]. For comparison with the results of section 3 we have extended the output plane to the far-field by means of the lens, L, in Figure 13a. This figure verifies that the measured and numerically calculated intensities of a simple test chirp grating in the ± 1 grating orders are of nominally rect-function form. This can also be shown formally by Fourier Transformation[23] and can be made physically plausible by invoking the linearity of the Fourier Transform. Thus the overall response (say in the + 1 grating order) is the sum of the responses of a number of subsections of the grating, each with its own local period, p(x). In fact, the fraction of the chirp grating effectively contributing to a point, P, in the centre of the response can be shown to be $\simeq N^{-\frac{1}{2}}$, where N is the space-bandwidth product of the grating ($N \simeq 100$ in the experimental device of Figure 13).

The principal difference between the responses of Figure 5 and those of Figure 13 is the dispersive nature of the latter. This arises because of the asymmetric structure of the chirp grating, the bilateral symmetry of the earlier apodised and withdrawal-weighted devices ensuring their linear phase characteristic[13]. In some applications it is important to maintain a linear phase response, and this can be achieved with chirp gratings by using a symmetrical up/down or "V"-chirp design. It is our intention to describe the overall behaviour of chirped optical diffraction gratings in more detail in a separate publication[24].

## 5. CONCLUSION AND DISCUSSION

In this paper we have described the use of apodisation, withdrawal-weighting and chirp weighting techniques to generalise the sinc-function response of a classical optical diffraction grating. However, as discussed in Appendix 1 other techniques derived from the field of SAW devices are equally applicable, for example the use of variable mark/space ratios, and the use of rotated slits. The former could be useful as it would combine two beneficial features of the individual techniques of apodisation and withdrawal-weighting, namely low inter-order sidelobe levels, and a sinc-function response in the v-direction of the output plane. The use of rotated slits could be interesting in that the response may have a natural tendency to be of rect-function form[25].
We have noted the close relationship between the spectral and spatial responses, and that each is related to the Fourier Transform of the aperture function. This Fourier Transform property is important as it ensures that, in principle at least, any (2-D) response can be obtained, and also defines the (2-D) structure needed to achieve it. In reality the performance is limited by various practical constraints, and these have been described in the case of nominally-rectangular responses (measured along the axis v = 0 in Figure 2) implemented with amplitude-only gratings. It has been shown that for

narrowband responses the 'detour-phase' technique can be employed to implement the necessary sign reversals as far as the ± 1 grating orders are concerned, but that this technique is ineffective in the zeroth and even orders. This conclusion is closely related to the well-known result in FT theory that a positive-definite function always has a peak response at the origin[26]. We have shown that for sharply truncated aperture functions there is a natural trade-off between the in-band and out-of-band responses, and described a curious phenomenon whereby the in-band response is smoothest when the (sinc-function) aperture is truncated half-way through a sidelobe. It should be emphasised that there exists a wealth of literature on superior truncation procedures, many developed for digital electronics, and that the results presented here should not be regarded as optimised in any sense. In particular, the article by Rabiner et al[27], describes such optimisation procedures for 1-D FIR (finite impulse response) filters, and additionally comments on asymmetric weighting, which results in more compact gratings at the expense of a non-linear phase response as in the case of the dispersive chirp gratings discussed in section 4. This article also discusses the design of two-dimensional filters, and is therefore relevant to an extension of the present investigations in which the response in the second dimension is exploited rather than studied as a feature of a 1-D response.

Any reader interested in the technique of apodisation can perform an extremely simple demonstration of the principles by overlaying a conventional diffraction grating with a square aperture whose edges are inclined at 45° to the slits; the response on the symmetry axis (v = 0) is then of sinc-squared form, displaying -26 dB close-in sidelobes, rather than the -13 dB sidelobes of a conventional sinc-function response. As discussed in Section 3 such an apodised grating also shows a strong off-axis sidelobe structure.

Concerning applications, responses of the type described here may be of use in certain forms of spectroscopy (eg Raman) to exploit the very low sidelobe levels realisable (-60 dB?) and/or the inherent notch-filter capability of the technique. Another such application is in wavelength division multiplexing (WDM), especially if 'point' detectors are mandatory, eg to handle large electrical bandwidths. Nominally rect-function responses themselves could be of value in communications systems employing WDM in which the (laser) frequencies are not precisely known beforehand, or which drift with time, temperature, etc. Following the successful exploitation of SAW devices as waveform generators[6-8], we speculate that weighted gratings could also be used to generate sophisticated optical waveforms, eg when 'impulsed' with sub-picosecond optical pulses. They could also be used as matched filters for such waveforms, or as group delay equalisers etc.

In the spatial domain output spots of nominally rect-function form with low sidelobe levels could be highly desirable to minimize inter-channel cross-talk in various optical computing and interconnection schemes[28]. However the issue of efficiency discussed below appears to make the use of volume (phase-) holography more attractive for this purpose at present. A disadvantage of the free-space amplitude-only structures described in this paper is their inherently low efficiency[29]. This would not be a problem, however, if our weighting techniques were employed in other grating structures such as reflective gratings in planar optics[30] and fibre optics[31]. These may or may not be operated in the FT mode. In such structures the incident light encounters many grating elements in series and the absence or weakness of particular reflecting elements does not incur a loss of optical power, but simply causes stronger illumination of succeeding elements. Of course, one must always be careful to ensure that the spectrum of such gratings does not allow phase-matching to unwanted modes in the medium itself, or in the surrounding free space, as this could deplete the required response and/or generate spurious illumination.

ACKNOWLEDGEMENT

It is a pleasure to acknowledge the assistance of Mike Hazell in the early stages of this work, and the skill of George Gibbons in producing the gratings.

REFERENCES


1. F A Jenkins and H E White, "Fundamentals of Optics", McGraw-Hill, New York, 1957.

2. E Hecht and A Zajac, "Optics", Addison-Wesley, 1974.

3. M C Hutley, "Diffraction Gratings", Academic Press, 1982.

4. R Petit (Ed), "Electromagnetic Theory of Gratings", Topics in Current Physics 22, Springer-Verlag, 1980.

5. Strictly one should distinguish between the frequency (or wavelength) response at a fixed detector location, and the spatial (or angular) response at a fixed optical wavelength. However the response is a function of the product k sin $\theta$ (where $k = 2\pi/\lambda$; $\theta$ is indicated in Figure 1a), so by fixing k or sin $\theta$, the response in the other variable (ie sin $\theta$ or k) takes the same form, eg a sinc function for simple gratings. Sin $\theta$ is usually small enough to be approximated by $\theta$. We shall have occasion to consider both responses in this paper.

6. H Matthews (Ed), "Surface Wave Filters", Wiley, New York, 1977.

7. D P Morgan, "Surface Wave Devices for Signal Processing", Elsevier, New York, 1985.

8. M F Lewis, C L West, J M Deacon and R F Humphreys, "Recent Developments in SAW Devices", IEE Proceedings 131A (1984) pp 186-214.

9. M F Lewis, "A Versatile SAW Filterbank Derived from the Optical Diffraction Grating", IEEE Trans UFFC-33 (1986) pp 681-691.

10. J H Elliott, R B Stokes and K H Yen, 'SAWFAST: A SAW Diffraction Channeliser", Microwave Journal, Sept 1986, pp 177-186.

11. J W Goodman, "Introduction to Fourier Optics", McGraw-Hill, 1968.

12. B J Thompson in Ch 2 of "Optical Data Processing", Topics in Applied Physics 23, Springer-Verlag, 1978.

13. R Bracewell, "The Fourier Transform and its Applications", McGraw-Hill, New York, 1965.

14. A G Hodkin and J M Bagshaw, "Anisot-opic Acousto-optic Interactions from Bulk and Surface Acoustic Waves", Proc 1983 IEEE Ultrasonics Symposium, pp 459-462.

15. P Hartemann and E Dieulesaint, "Acoustic Surface Wave Filters", Electronics Letters 5 (1969), pp 657-8.

16. B R Brown and A W Lohmann, "Complex Spatial Filtering with Binary Masks", Appl Optics 5 (1966) pp 967-969.


17. This description is not quite equivalent to the normal use of "apodization" in optics, but is made by direct analogy with SAW device technology.

18. It is unfortunate that the term 'sidelobe' is conventionally used in either domain. It is hoped that the context will suffice to avoid any confusion here.

19. E M Garber and H A Haus, "Synthesis of High Performance SAW filters with non-uniformly spaced fingers", Proc 1983 IEEE Ultrasonics Symposium pp 27-32.

20. M B Shulz, M G Holland and L Davis, "Optical Pulse Compression Using Bragg Scattering by Ultrasonic Waves", App Phys Let 11 (1967) pp 237-240.

21. J H Collins, E G H Lean and H J Shaw, "Pulse Compression by Bragg Diffraction of Light with Microwave Sound", App Phys Lett 11 (1967) pp 240-242.

22. J B Merry and L Bademian, "Acousto-optic Laser Scanning", Proc. SPIE 169 Laser Printing (1979) pp56-59.

23. E Dieulesaint and D Royer, "Elastic Waves in Solids", Wiley 1980, Ch 9.

24. M F Lewis and C L West, "A Theoretical and Experimental Investigation of Linear and Nonlinear Focussing Chirped Optical Diffraction Gratings", RSRE Memorandum No. 4129, 1988.

25. A P van den Heuvel, "Use of Rotated Electrodes for Amplitude Weighting in Interdigital Surface Wave Transducers", App Phys Lett 21 (1972) pp 280-282.

26. A Papoulis, "The Fourier Integral and its Applications", McGraw-Hill, 1962, Ch 11.

27. L R Rabiner, J H McClellan and T W Parks, "FIR Digital Filter Design Techniques Using Weighted Chebyshev Approximation", Proc IEEE 63 (1975) pp 595-610.

28. H J Caulfield, J A Neff and W T Rhodes, "Optical Computing: The Coming Revolution in Optical Signal Processing", Laser Focus/Electro-optics, November 1983, pp 100-110.

29. J L Horner, "Light Utilisation in Optical Correlators", Appl Opt 21 (1982) pp 4511-4.

30. A C Livanos, A Katzir, A Yariv and C S Hong, "Chirped-grating demultiplexers in dielectric waveguides", App Phys Lett 30 (1977) pp 519-521. See also the Proceedings of the IEEE International Workshop on "Integrated optical and related technologies for signal processing", Firenze, Italy, Sept 10-11 (1984).

31. I Bennion, D C J Reid, C J Row and W J Stewart, "High-reflectivity monomode-fibre grating filters", Electronics Letters 22 (1986) pp 341-3.

## APPENDIX 1

The purpose of this appendix is to provide a succinct account of the basics of SAW devices and their weighting techniques. Fuller descriptions are given in references 6-8. A 2-port SAW device is shown schematically in Figure A1(a) and comprises a pattern of metallic electrodes formed photolithographically on the polished surface of a piezoelectric substrate such as quartz or $LiNbO_3$. When an input rf voltage is applied to the terminals of the rhs (apodised) transducer, the electric fields in each gap generate rf strains at the substrate surface through the (inverse) piezoelectric effect. Such time-varying strains travel away from each source as wavelets at the velocity of SAW, V, which is typically 3000 m/s. Since the sources have apertures A(x) which are invariably much greater than the SAW wavelength, they act as line sources emitting SAW radiation to the left and right in essentially plane wave form. We are only concerned with SAW propagation to the lhs which is intercepted by the broadband output IDT wherein it generates an output voltage by the (direct) piezoelectric effect. If the input transducer is impulsed by a voltage waveform approximating $\delta(t)$, each source responds by emitting a short mechanical pulse which for the moment we will also assume to be of $\delta$-function form. Thus the net impulse response of the device, h(t), emerging from the output transducer takes the form

$$h(t) \propto \sum_n A_n(x)\ \delta(t-x_n/V) \qquad (A1)$$

The frequency response, H(f) is the Fourier Transform of h(t),

$$H(f) = \int_{-\infty}^{\infty} h(t)\ \exp{-j2\pi ft}\ dt \propto \sum_n A_n\ \exp{-j2\pi fx_n/V} \qquad (A2)$$

If all the $A_n$ are equal, and the $x_n$ are periodic with interval $\Delta x$, Equation (A2) takes the form of a series of sinc-function frequency responses (harmonics) repeated at intervals $\Delta f = V/\Delta x$. In reality the electrode-pairs of Figure A1(a) do not act as ideal $\delta$-function sources but have a frequency response (element factor) of their own which depends on the details of the electrode structure, eg on the mark/space ratio. Many structures in common use are shown in Ref 8, Figure 5. The element factor determines the relative strengths of the harmonic responses of the IDT, and is analogous to the effect of a finite slit width in diffraction gratings, which of course determines the relative strengths of the grating orders. The principal difference in behaviour is that SAW devices do not respond at their zeroth or even harmonics. The impulse response of the device of Figure A1(a), filtered to remove higher harmonics, is shown in Figure A1(b), as it would appear on a CRO, and is seen to resemble closely the physical construction of the IDT. This feature is valuable in providing physical insight into the design and operation of SAW devices. It may be noted that strictly speaking the output field of the IDT is 2-dimensional, but that the use of a large-aperture output IDT rejects components with $k_y \neq 0$. Similarly, if both the input and output IDTs are apodised it becomes desirable to use an additional component, the multistrip coupler, to restore the condition $k_y \simeq 0$, Ref 8, Figure 10. Only recently has this 2-dimensionality been seriously exploited to provide a multi-port SAW (filterbank) capability[9,10]. This aspect of SAW is closely analogous to the 2-dimensionality of the output field of an optical diffraction grating. Countless responses have been achieved in SAW devices by varying the $A_x$ and x in various ways. Some of the weighting schemes devised for SAW IDTs are illustrated schematically in Figure A2, and are largely self-explanatory. Each of these is applicable to optical diffraction gratings except the dog-leg scheme in which weighting is achieved through capacitive division of the applied voltage.

## APPENDIX 2

The purpose of this Appendix is to provide a succinct derivation of the modified Fourier transform relationship obtaining in the experimental arrangement of Figure 1(b) using the paraxial approximation. The argument follows the approach and sign convention of Thompson[12] and is one-dimensional for simplicity. In Figure A3, the components of Figure 1(b) are redrawn to include the virtual source, S, of which the central point, I, in the output plane is an image in the absence of the diffraction grating in the input plane. Thus all rays from S to I undergo the same overall phase-shift, so that the relative field at some point, $x_1$, in the input plane is

$$\psi(x_1) = \exp(-jkm) \tag{A3}$$

The - sign in the exponent indicates the conjugate of the normal phase shift from $x_1$ to I, because we have traced back from I to obtain the phase at $x_1$. In the presence of the grating the field in the input plane is given by the transmittance of the grating, g(x), modified by the phase factor in Eqn (A3). Thus by Huygen's principle the field in the output plane is given by

$$\varphi(u) = \int dx[g(x)\ \exp(-jkm)]\ \exp(jks) \tag{A4}$$

where $m^2 = d^2 + x^2$ and $s^2 = d^2 + (u-x)^2$. In the small angle approximation

$$\left.\begin{aligned} m &\simeq d + x^2/2d \\ s &\simeq d + (u-x)^2/2d \\ m-s &\simeq (2xu-u^2)/2d \end{aligned}\right\} \tag{A5}$$

Making these substitutions in Eqn (A4) gives

$$\varphi(u) = \exp(jku^2/2d)\int dx\ g(x)\ \exp(-jkxu/d) \tag{A6}$$

From Eqn (A6) it is seen that $\varphi(u)$ is still a measure of the Fourier transform of g(x), but modified by the phase factor $\exp(jku^2/2d)$, which is of no practical consequence because of Eqn (2). In addition the factor 'd' in the exponent under the integral sign shows that the scale of the output field is modified in proportion to d. In Figure 1(b) this feature is exploited to fill the camera aperture with relevant data.

Figure 1

(a) Schematic plan view of the conventional arrangement for measuring the response of a diffraction grating

(b) The modified arrangement used in much of the present work

Figure 2

A well-known configuration for obtaining the FT of an input aperture function f(x,y) in the output plane (u,v). For reasons of economy the input function illustrated is a conventional diffraction grating illuminated by a monochromatic plane wave, and with spatial dimensions labelled as in the text. The number of slits, N, is closely equal to a/p.

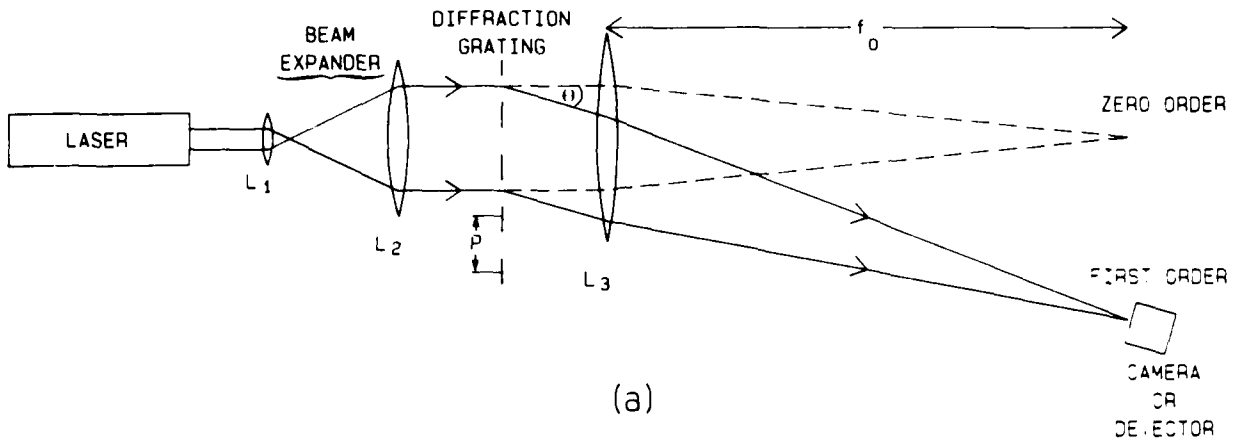


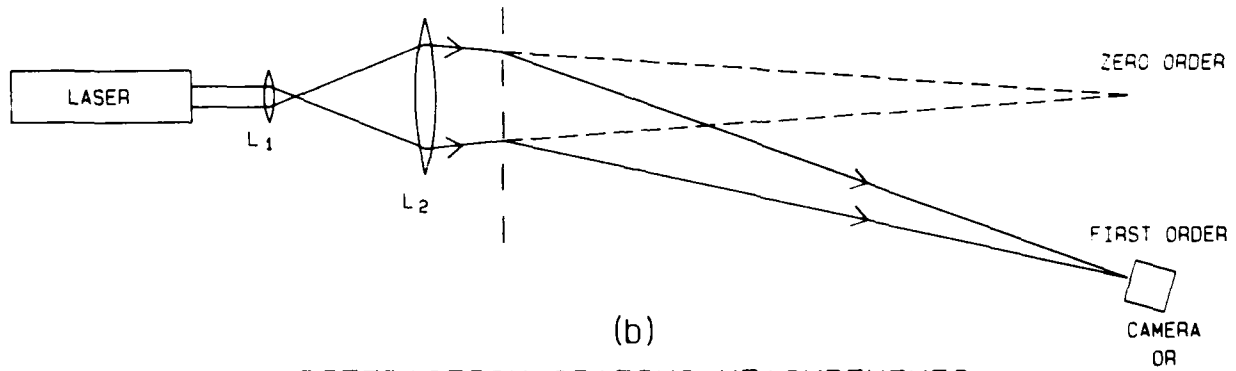


FIGURE 1. DIFFRACTION GRATING MEASUREMENTS

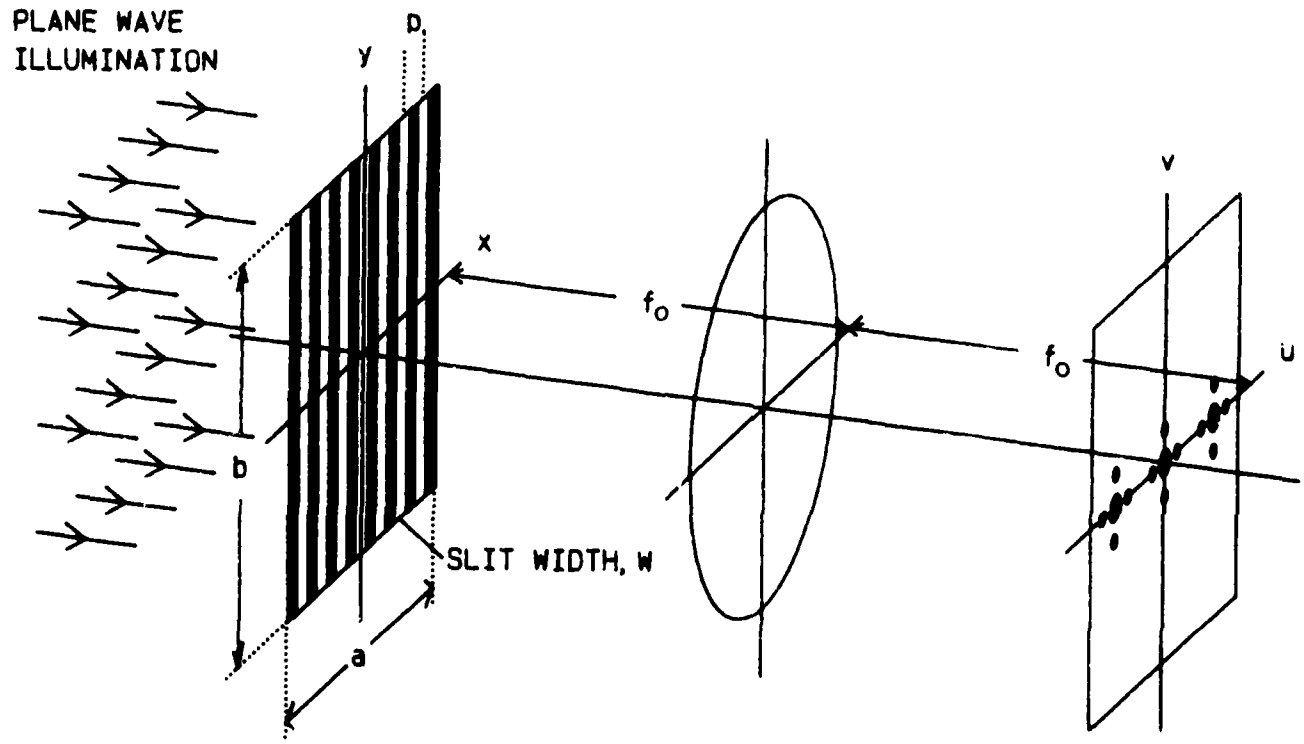


FIGURE 2.

Figure 3

Measured (rhs) and calculated (lhs) responses of a conventional optical diffraction grating in its first order. The instantaneous dynamic range of 45 dB was obtained using the heterodyne technique described in the text.

Figure 4

Schematic diffraction gratings incorporating truncated sinc-function weighting. (a) An apodised grating with m = $1\frac{1}{2}$ sidelobes on either side of the main lobe. The inset illustrates the half-period step used to implement the sign reversals between sidelobes. (b) A withdrawal-weighted grating with m = 3 sidelobes on either side of the main lobe.

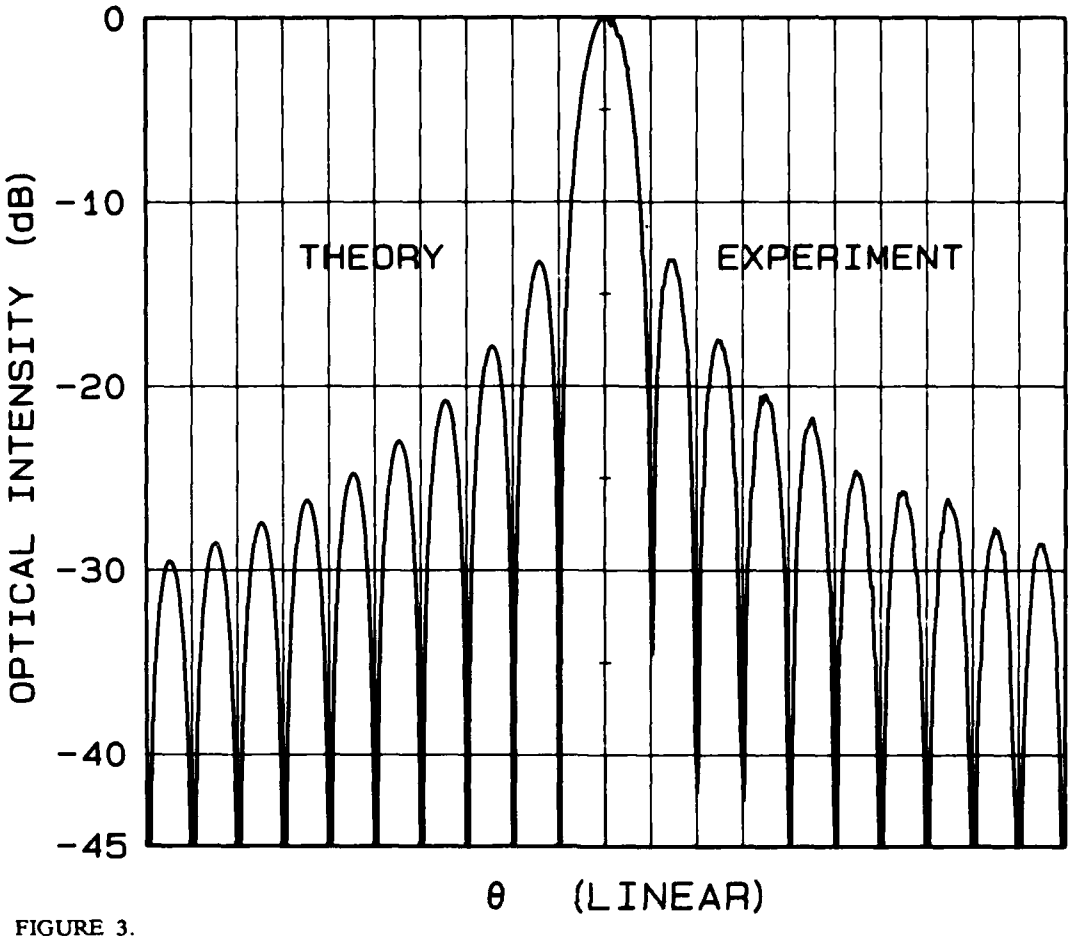
0
-10
-20
-30
-40
-45
OPTICAL INTENSITY (dB)
THEORY
EXPERIMENT
θ (LINEAR)

FIGURE 3.

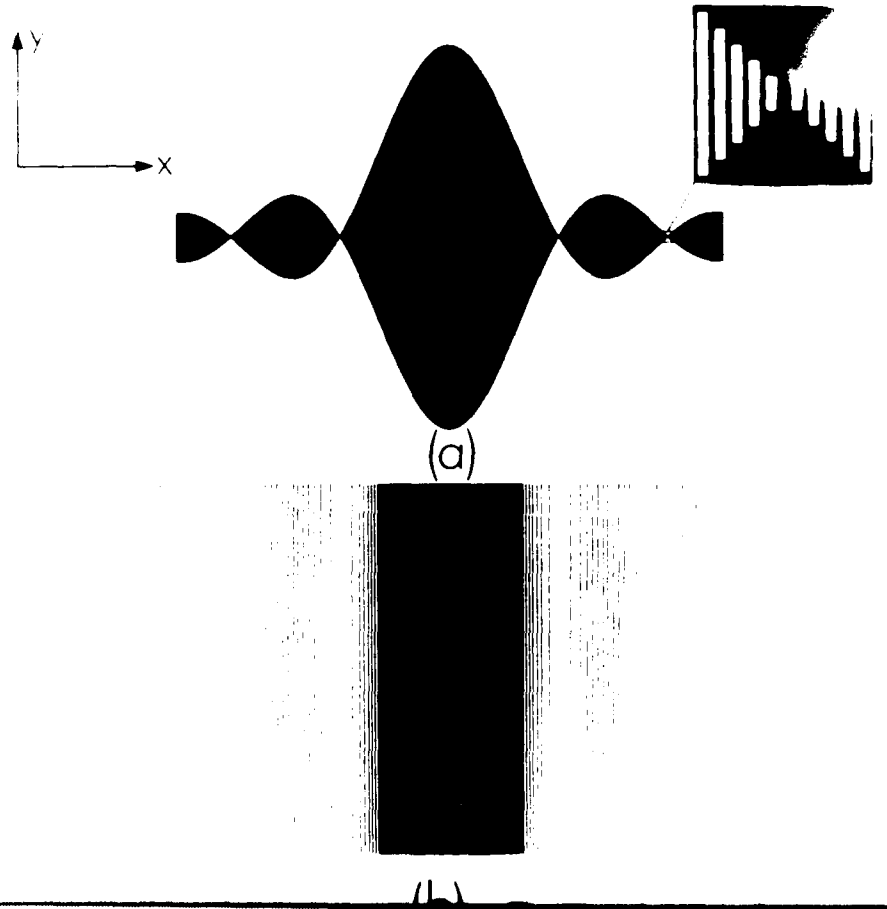
Y
X
(a)

Figure 5

Measured and calculated responses of weighted optical diffraction gratings along the symmetry axis, v = 0 of the output plane,

(a) apodized grating with integer numbers of sidelobes on either side of the main lobe;

(b) apodized grating with half-integer numbers of sidelobes.

(c) withdrawal-weighted grating with integer numbers of sidelobes.

(d) withdrawal-weighted grating with half-integer numbers of sidelobes.

Note the close agreement between experiment and theory and between apodized and withdrawal-weighted responses.

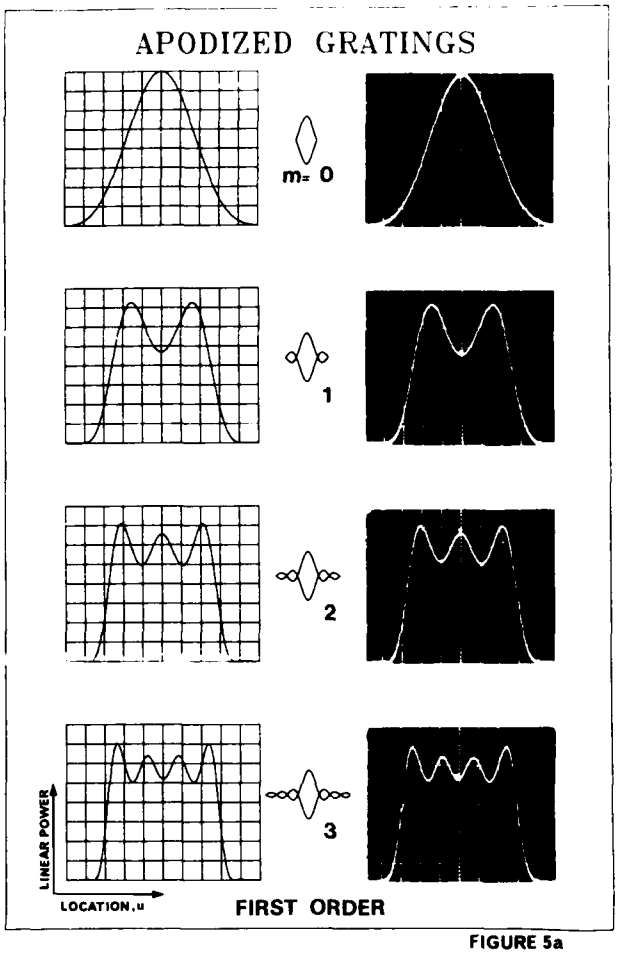


FIGURE 5a

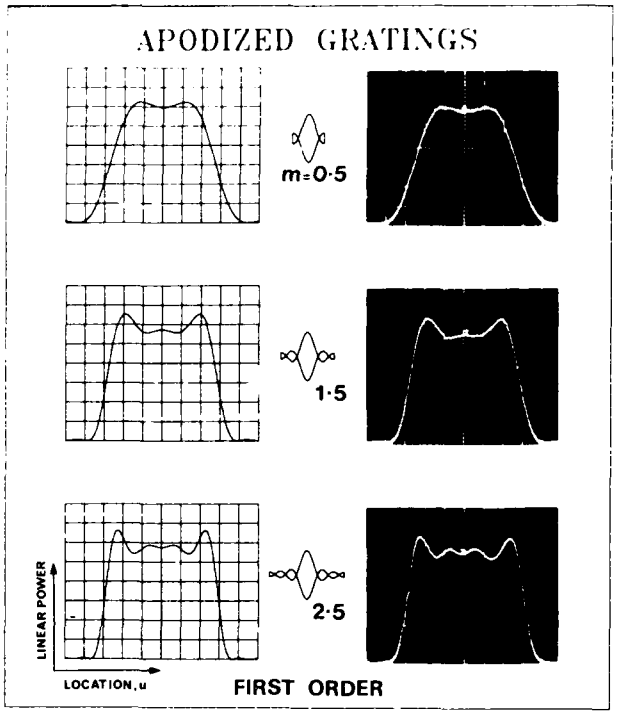


FIGURE 5b

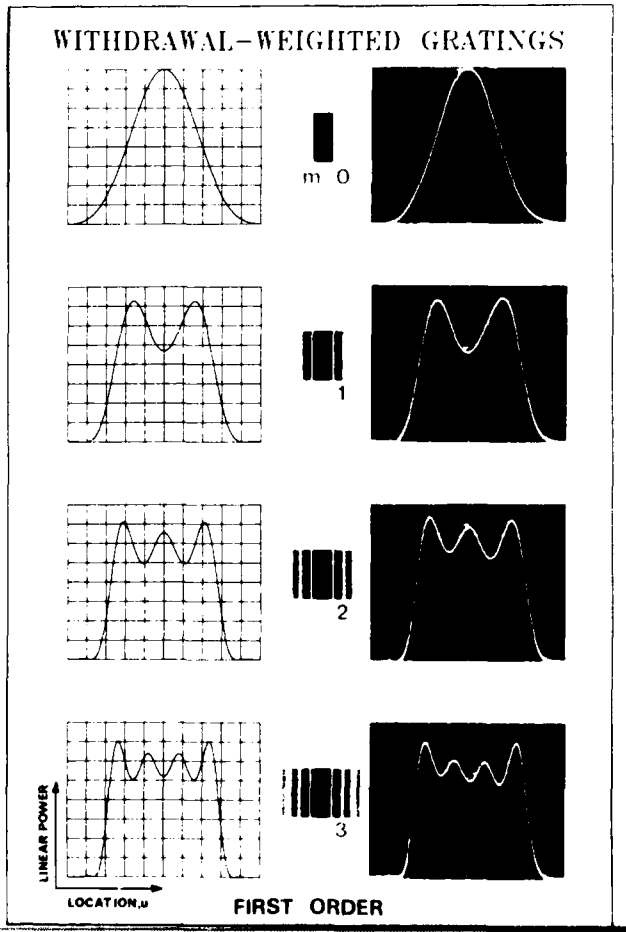


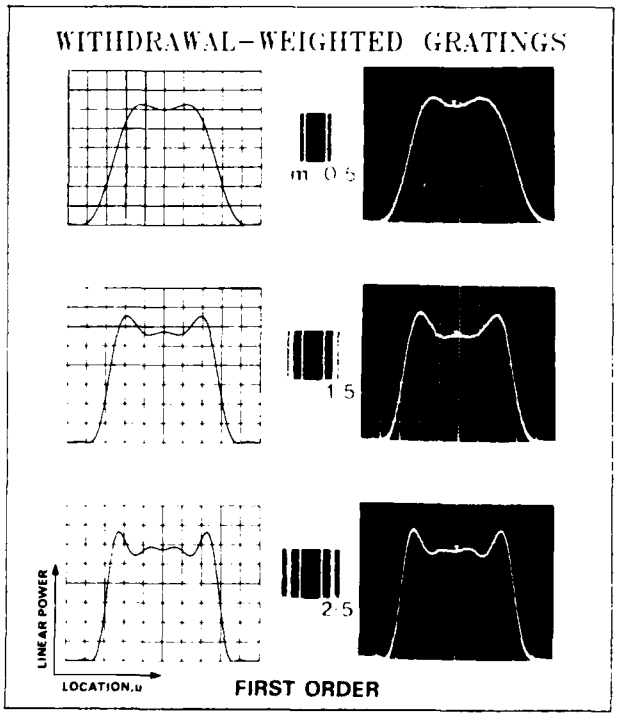


FIGURE 5d

Figure 6

Calculated (a–c) and measured (d–f) responses of 3 apodised gratings of Figure 5 plotted on a dB scale. The particular results shown derive from gratings with low values of $m$ (viz 0, $\frac{1}{2}$, 1) because these display the greatest trade–off between the in–band and out–of–band responses.

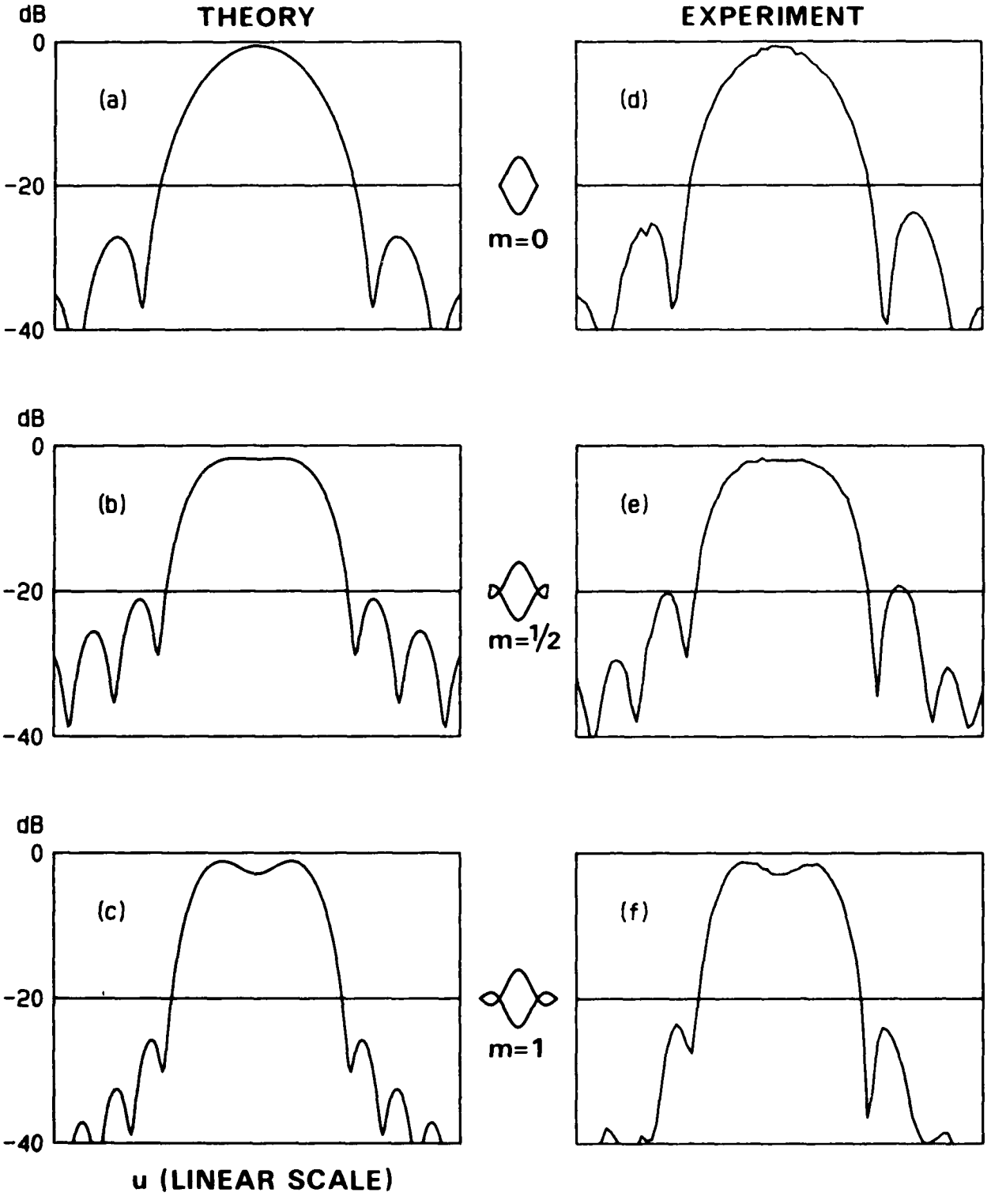


FIGURE 6.

Figure 7

This illustrates graphically the origin of the behaviour in Figures 5 and 6. The pairs of short horizontal arrows in (b), (d) and (f) indicate that the functions extend to $\pm \infty$. The double-headed vertical arrows indicate a Fourier transform relationship, e.g. between functions (a) and (d). (g) and (i) illustrate the convolution process in-band and out-of-band respectively for a grating with an integer value of m. (h) and (j) illustrate corresponding stages of the convolution process for gratings with a half-integer value of m.

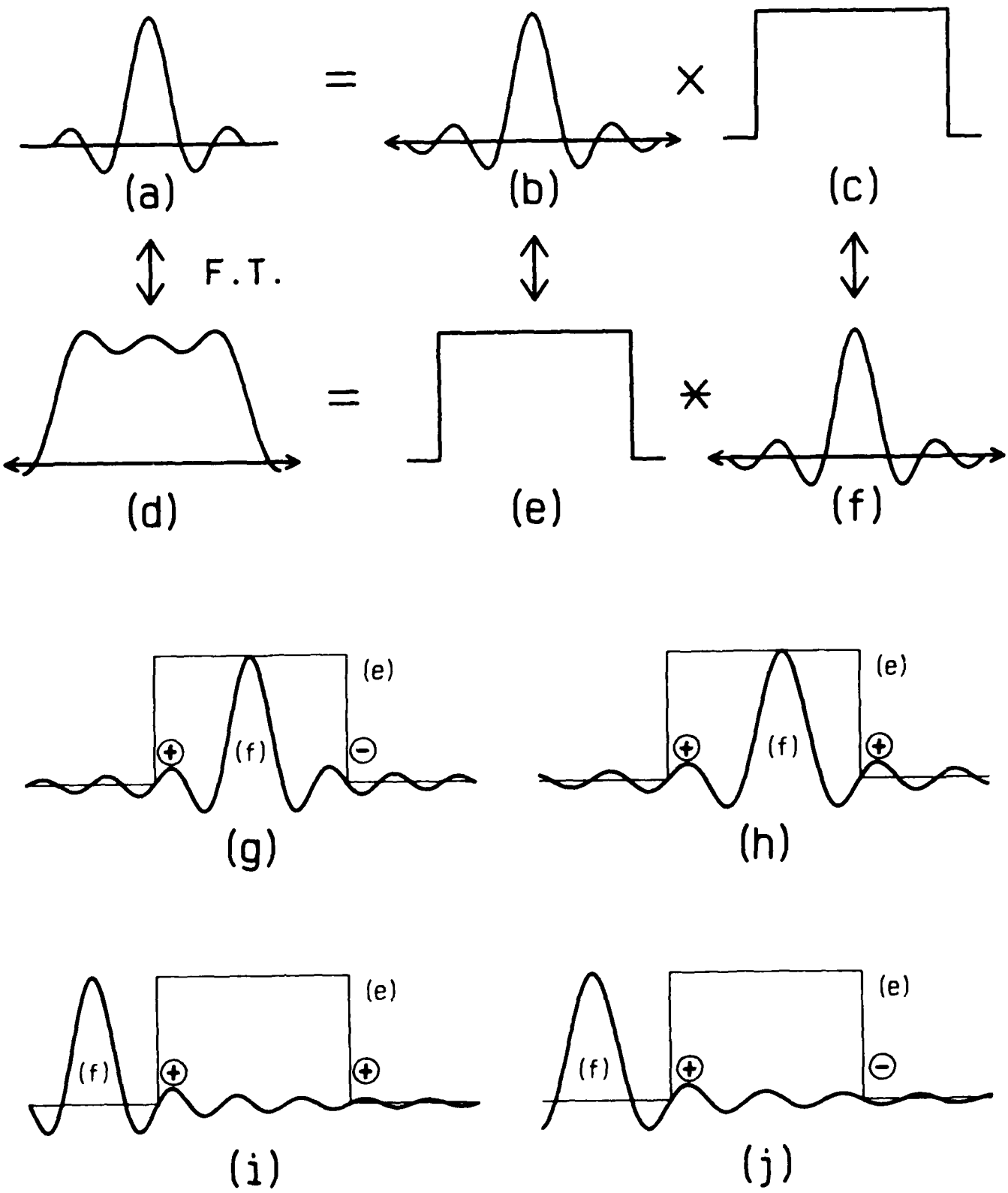


FIGURE 7.

Figure 8

Experimental and theoretical responses of (a) apodized and (b) withdrawal-weighted gratings showing the 2-D output plane, (u,v) in perspective and illustrating the off-axis sidelobe structure. The off-axis responses for half-integer sidelobe patterns are similar to those given for integer sidelobe patterns and are not shown here. Note that the variation for the withdrawal-weighted gratings in the v-direction is of sinc-function form

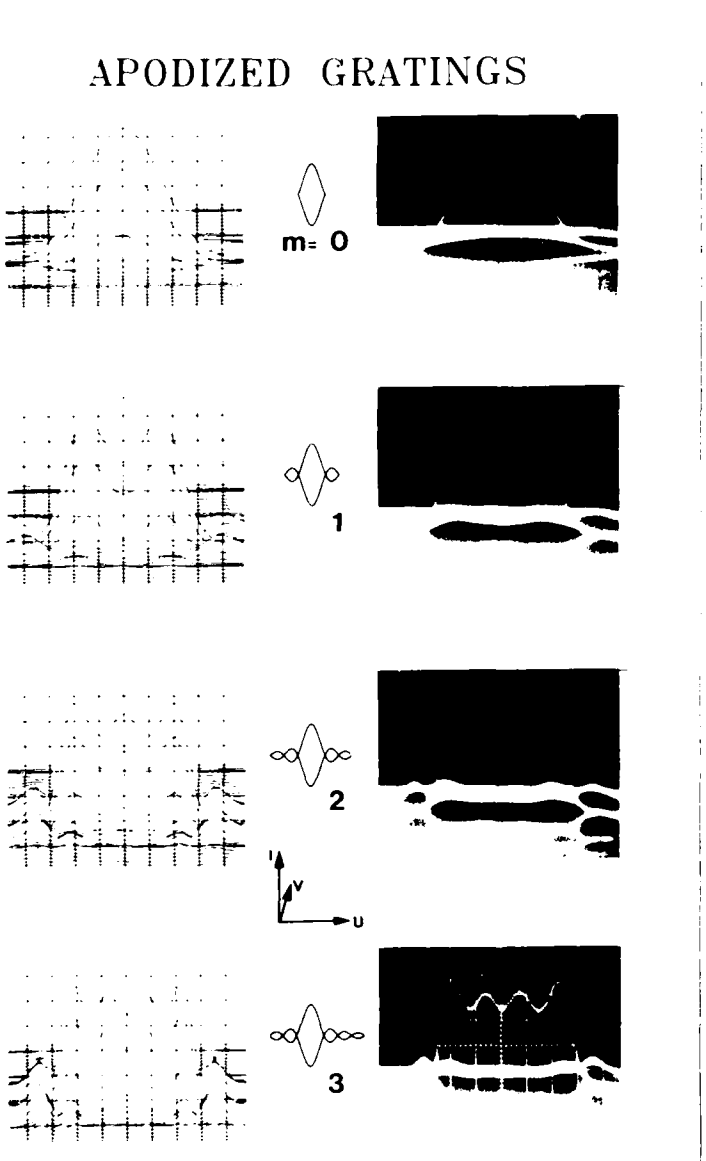


FIGURE 8a

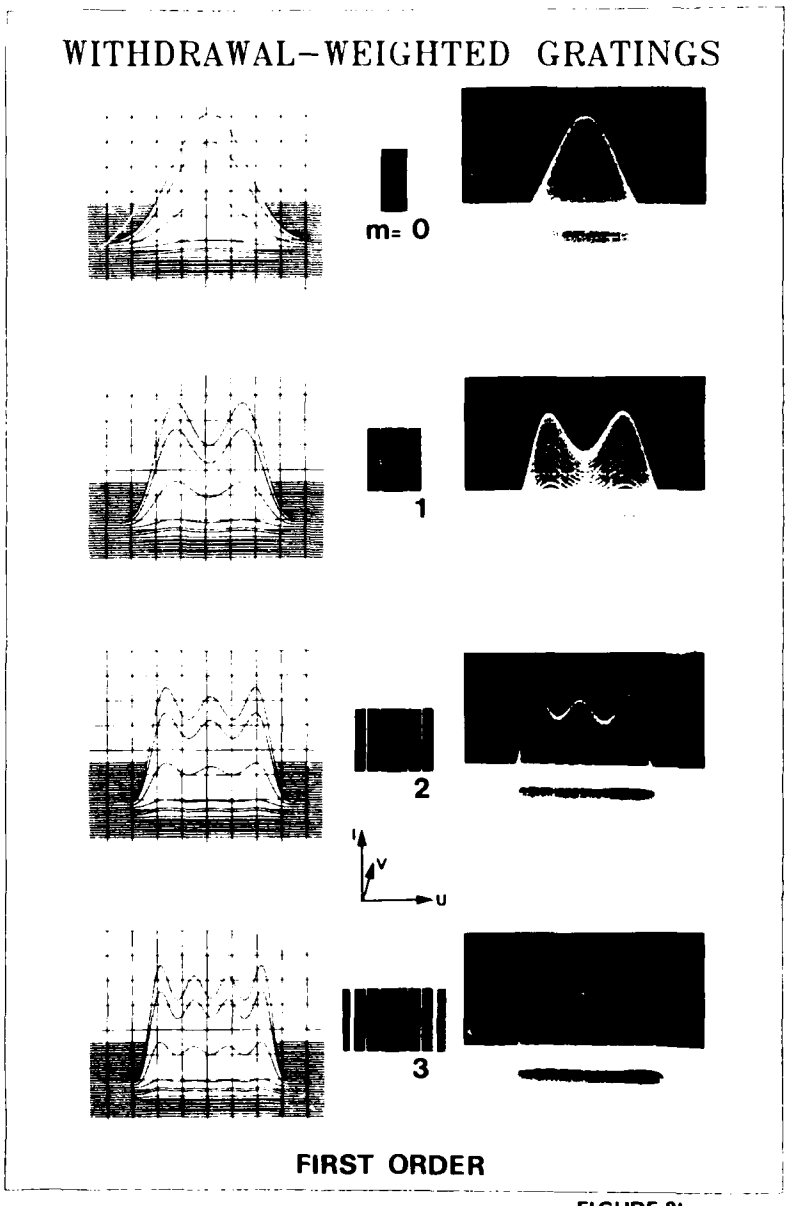


FIGURE 8b

Figure 9

(a) shows the response of an apodised grating (with m = 3) in the +1 grating order, cf Figure 5a.

(b) shows that the corresponding response in the zeroth order is much narrower. This arises because all slits are in phase, effectively extending the width of the main lobe to the full grating aperture. Although this response is close to calculation it is slightly distorted by optical 'breakthrough' due to the finite optical density (OD = 3.5) of the opaque area of the mask.

(c) shows the much more severe distortion of the zeroth order response of a mask with background OD = 2.5.

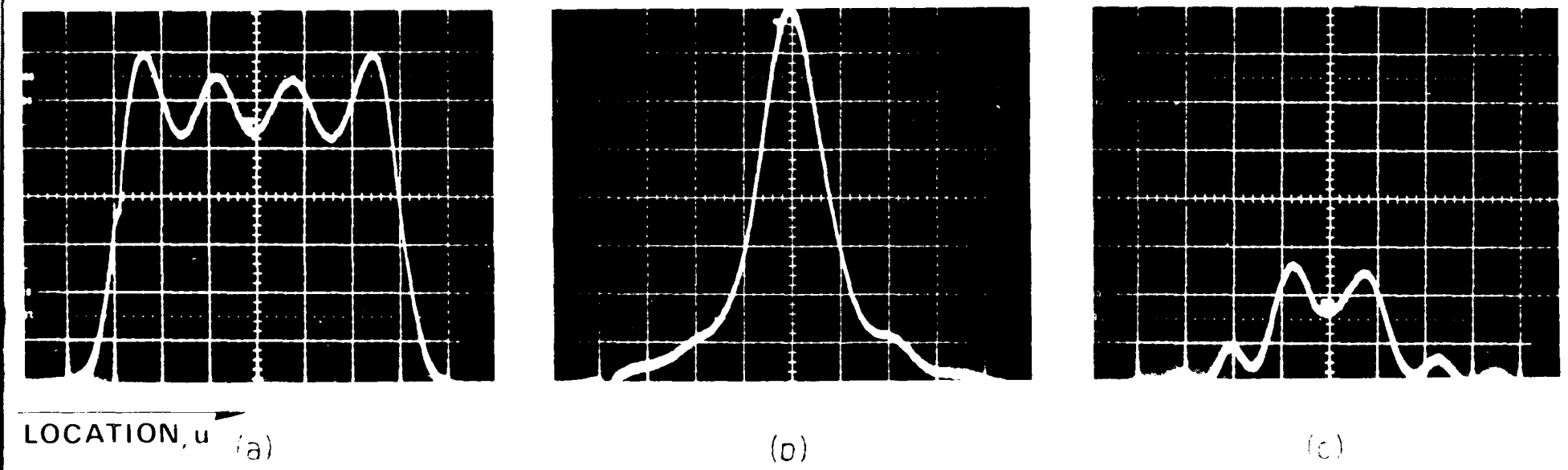


FIGURE 9.

Figure 10

(a) Illustrates the origin of the narrow even-order responses. In the even orders the detour phase due to the half-period steps (shown here and in the inset to Figure 4(a)) is an integer multiple of $2\pi$, and is therefore totally ineffective. It may also be noted that even in the odd orders this phase reversal procedure is only perfectly effective at the centre frequencies (wavelengths). However, it is adequate to realise narrow-band responses such as those described in this paper.

(b) Experimental confirmation of the difference between odd and even orders of a diffraction grating which has displaced slits to realise a $\lambda/2$ pathlength shift in the first order. The data shown was the output from a TV camera for various orders of an apodized diffraction grating with m = 2. The relative intensity shows the peak signal strength relative to that of the zeroth order. Note that for an accurately defined 1:1 mark/space ratio all the even orders, except the zeroth, will have zero intensity. In practice weak responses are observed due to minor imperfections in manufacture.

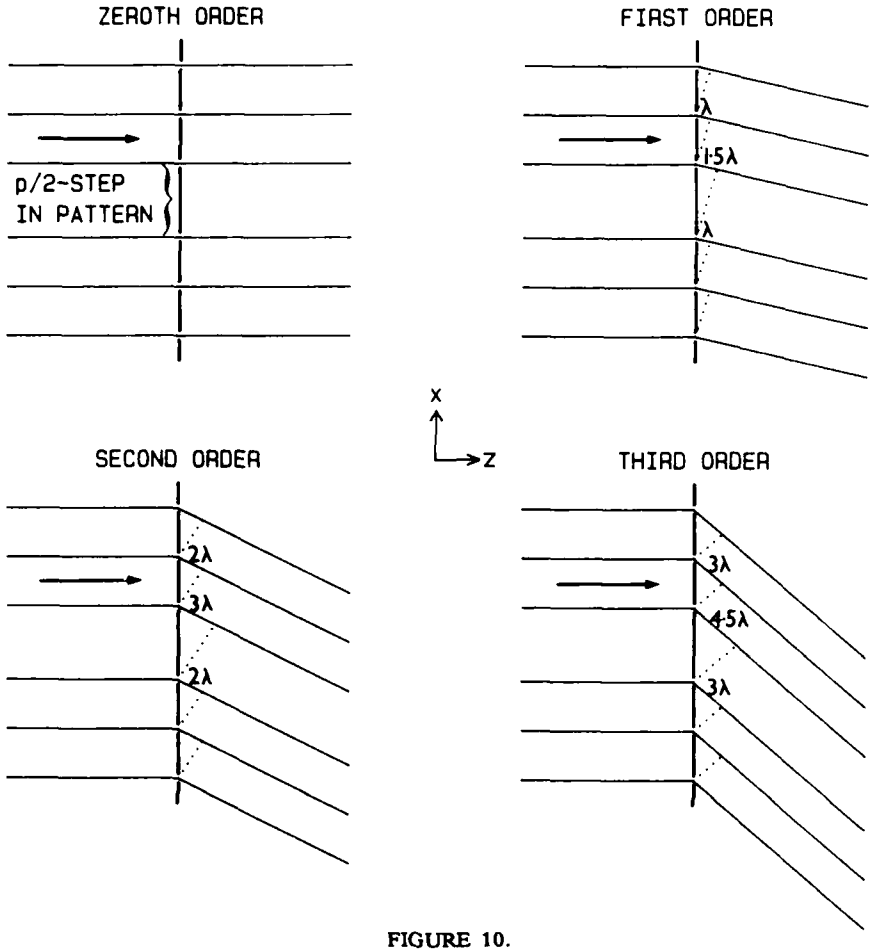


FIGURE 10.

## DIFFRACTION ORDERS OF AN APODIZED DIFFRACTION GRATING WITH m=2 SHOWING THE DIFFERENCE BETWEEN THE BEHAVIOUR IN ODD AND EVEN ORDERS

| ORDER | 0 | 1 | 2 | 3 | 4 | 5 |
|---|---|---|---|---|---|---|
| RELATIVE INTENSITY (dB) | (0) | (-5) | (-25) | (-15) | (-25) | (-20) |

FIGURE 10b

Figure 11

(a)-(c) Responses of an apodised grating with m = 3 when illuminated by an Argon ion laser operating in its 'all lines' mode. (a) the 2-D output plane in perspective, (b) the response along the symmetry axis, v = 0 (the ordinates are linear in optical power) and (c) the TV monitor display. Five discrete lines with wavelengths ranging from 476.5 to 514.5 nm are clearly visible.

(d) Responses of a withdrawal-weighted grating with m = 3 when illuminated by an Argon ion laser operating in its 'all lines' mode: TV monitor display.

(c) and (d) demonstrate the difference between the two weighting schemes with regard to off-axis structure. In particular, note that it would not be possible to use a detector extended in the v-direction for the apodized gratings whereas this would be acceptable for the withdrawal-weighted gratings.

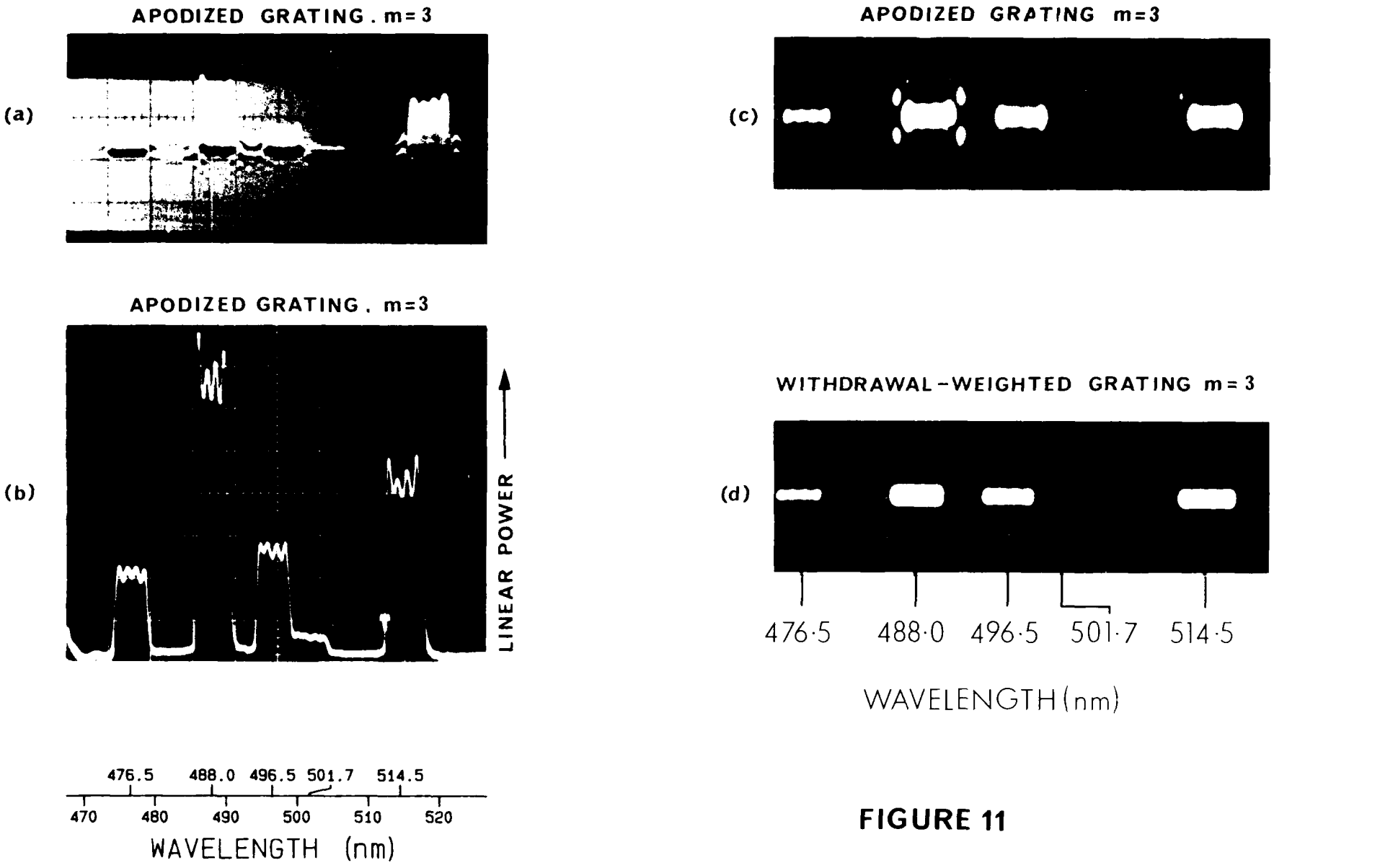
APODIZED GRATING . m=3
(a)
APODIZED GRATING . m=3
(b)
LINEAR POWER
476.5 488.0 496.5 501.7 514.5
470 480 490 500 510 520
WAVELENGTH (nm)
APODIZED GRATING m=3
(c)
WITHDRAWAL-WEIGHTED GRATING m=3
(d)
476·5 488·0 496·5 501·7 514·5
WAVELENGTH (nm)

**FIGURE 11**

Figure 12

This compares the behaviour of apodised and withdrawal-weighted gratings between orders. (a) and (b) show respectively the calculated and measured responses of a withdrawal-weighted grating (with m = 3) over a range covering the zeroth and first grating orders. (c) and (d) show the corresponding responses for apodised gratings. The fine structure in (c) is of no consequence; it arises from the sampling process in the numerical computation procedure.

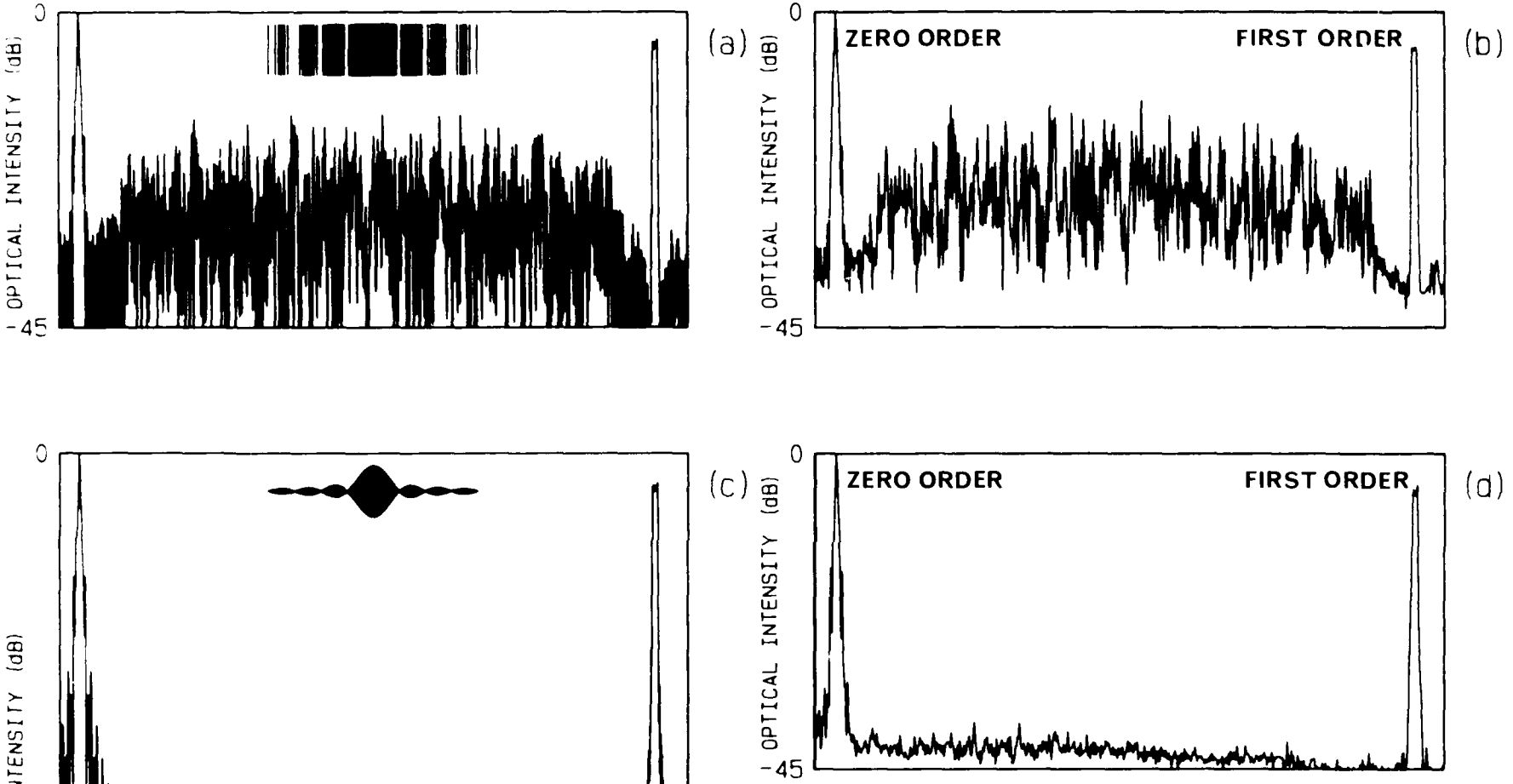


FIGURE 12.

Figure 13

(a) shows a plan view of the formation of the far-field Fraunhofer pattern of a dispersive grating, with its approximately rectangular response in the ± 1 grating orders. Most previous interest in such gratings has arisen from the formation of the focus F.

(b) experimental responses in the zeroth and +1 grating orders confirming the calculated behaviour in (a).

The grating comprised 500 slits with periods ranging from 14.89 $\mu$m to 17.41 $\mu$m and had a focal length of 160 cm. Although the peak intensity of the zeroth order is $\approx$ 50x greater than that of the first order they are shown equal for clarity in the calculated responses in (a).

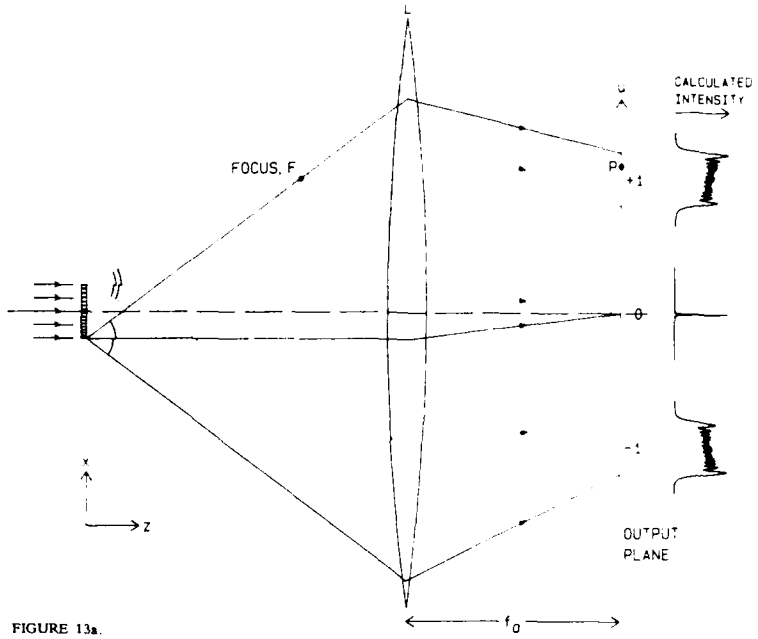


FIGURE 13a.

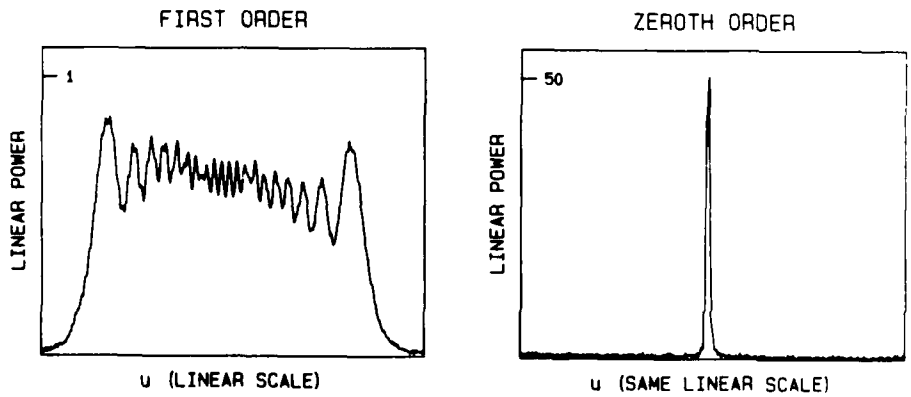


FIGURE 13b

Figure A1
(a) A schematic apodised SAW interdigital transducer in which the variable overlap A(x) introduces weighting.
(b) The impulse response of this IDT, filtered to remove harmonics higher than the fundamental.

Figure A2
Schematics of nine designs of SAW IDT. Each of these can be implemented in optics, except (e), in which weighting is achieved by electrical circuit effects.

Figure A3
Structure used to derive the modified Fourier Transform properties of the experimental arrangement of Figure 1b.

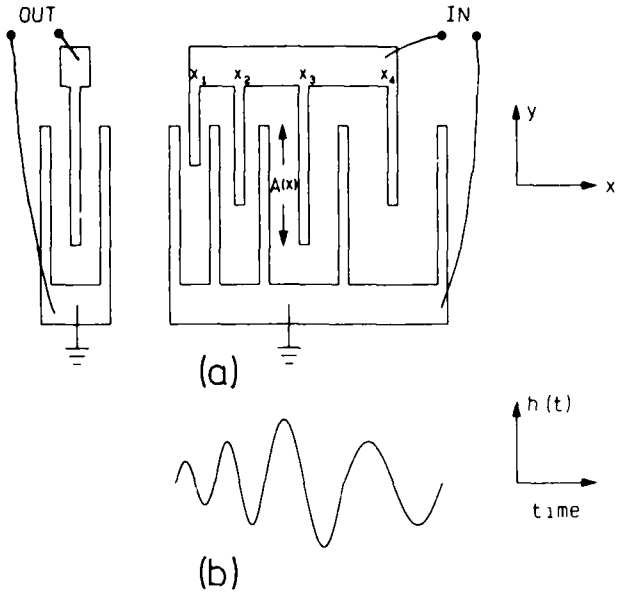


FIGURE A1.

SOME WEIGHTING SCHEMES DEVISED FOR SAW INTERDIGITAL TRANSDUCERS

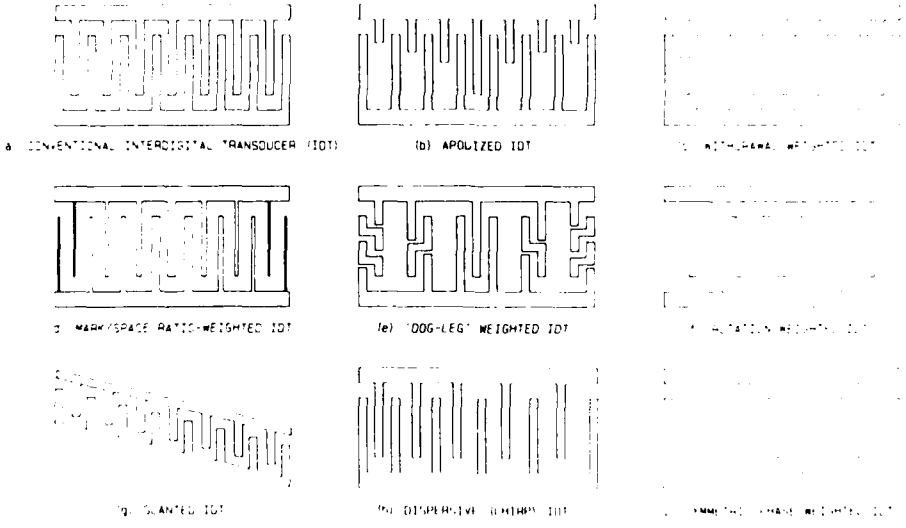


FIGURE A2

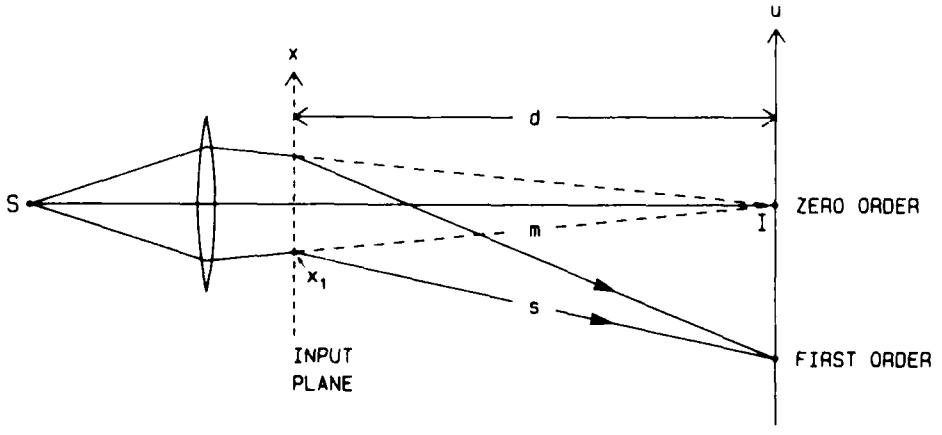


FIGURE A3.

DOCUMENT CONTROL SHEET

Overall security classification of sheet ..... UNCLASSIFIED .....

(As far as possible this sheet should contain only unclassified information. If it is necessary to enter classified information, the box concerned must be marked to indicate the classification eg (R) (C) or (S) )

| 1. DRIC Reference (if known) | 2. Originator's Reference | 3. Agency Reference | 4. Report Security Classification |
|---|---|---|---|
| | Memorandum 4128 | | Unclassified |

| 5. Originator's Code (if known) | 6. Originator (Corporate Author) Name and Location |
|---|---|
| 778400 | Royal Signals and Radar Establishment<br>St Andrews Road, Malvern, Worcestershire WR14 3PS |

| 5a. Sponsoring Agency's Code (if known) | 6a. Sponsoring Agency (Contract Authority) Name and Location |
|---|---|
| | |

7. Title

A THEORETICAL AND EXPERIMENTAL INVESTIGATION INTO THE USE OF SAW WEIGHTING TECHNIQUES IN OPTICAL DIFFRACTION GRATINGS

7a. Title in Foreign Language (in the case of translations)

7b. Presented at (for conference papers) Title, place and date of conference

| 8. Author 1 Surname, initials | 9(a) Author 2 | 9(b) Authors 3,4... | 10. Date | pp. ref. |
|---|---|---|---|---|
| Lewis M F | West C L | | 1988.03 | 26 |

| 11. Contract Number | 12. Period | 13. Project | 14. Other Reference |
|---|---|---|---|
| | | | |

15. Distribution statement

Unlimited

Descriptors (or keywords)

continue on separate piece of paper


Abstract

This Memorandum describes the behaviour of optical diffraction gratings which have been weighted in various ways analogous to those used in surface acoustic wave (SAW) devices. It is shown experimentally and theoretically that a wide variety of two-dimensional responses can be achieved by these means. In this study we have chosen to concentrate on quasi-rectangular responses, and we describe in some detail the factors that limit the performance achievable in practice. Some possible applications of these techniques in the spatial, temporal and spectral domains are mentioned. A succinct version of this Memorandum has been submitted to the journal "Applied Optics".